Mechanisms of Inward-Rectifier K^+ Channel Inhibition by Tertiapin-Q†

Weili Jin, Angela M. Klem, John H. Lewis, and Zhe Lu*

Department of Physiology, University of Pennsylvania, 3700 Hamilton Walk, Philadelphia, Pennsylvania 19104

Received May 25, 1999; Revised Manuscript Received July 22, 1999

ABSTRACT: Tertiapin-Q (TPN_Q) is a derivative of honey bee toxin tertiapin (TPN) whose methionine residue is replaced with a glutamine residue. TPN_Q inhibits the ROMK1 and GIRK1/4 inward-rectifier K^+ channels with affinities very similar to TPN. However, unlike native TPN, TPN_Q is nonoxidizable by air. The stability of TPN_Q allows us to investigate how it interacts with the targeted channels. We found that the interaction between TPN_Q and the ROMK1 channel is a bimolecular reaction, i.e., one TPN_Q molecule binds to one channel. The interaction surface in TPN_Q is primarily formed by its α helix rather than the β sheets with which scorpion toxins form their interaction surface. The mutagenesis studies on both the channel and TPN_Q together strongly suggest that to block the K^+ pore TPN_Q plugs its α helix into the vestibule of the K^+ pore, while leaving the extended structural portion sticking out of the vestibule into the extracellular media.

Tertiapin (TPN) is a small compact protein of twenty-one amino acids, originating from the venom of the honey bee (*1*, *2*). TPN was recently rediscovered based on its inhibitory activity against two members of the inward-rectifier K^+ channel family, the GIRK1/4 and ROMK1 channels (*3*). TPN inhibits these channels with nanomolar affinity and would be a very useful tool for studying the inward-rectifier K^+ channels. However, methionine residue 13 in TPN can be oxidized by air and the oxidation hinders its binding to the targeted channels, making its study difficult (*3*, *4*). Interestingly, a non-air-oxidizable TPN derivative, called TPN_Q, in which the methionine residue is replaced by glutamine, inhibits the GIRK1/4 and ROMK1 channels with affinities very similar to TPN (*4*). Like TPN, it also does not inhibit the IRK1 channel. Thus, TPN_Q functionally resembles native TPN in both affinity and specificity—but is stable.

Two other toxins, apamin and the mast cell degranulating peptide, were previously purified from honey bee venom for their inhibitory activity against the voltage- and/or Ca^{2+}-activated K^+ channels (*5*, *6*). Neither of these two toxins effectively blocks the inward-rectifier K^+ channels blocked by TPN (*3*). The three-dimensional structures of apamin and TPN have been solved using NMR-spectroscopic techniques (*7*, *8*). Although these two toxins share minimal homology in their amino acid sequences, they have very similar backbone structures. Each of the structures consists of an α helix and a type-I reverse turn. A loop partially formed by an extended β sheet connects the turn and the helix. Four cysteine residues within the polypeptide chain form two disulfide bonds. The main difference between the two structures is the relative position of the connecting loop and the α helix, resulting from the existence of an extra residue in TPN's connecting loop. It is unclear whether the dramatically different inhibitory activities of TPN and apamin against the targeted channels is due to the presence of different residues in their interaction surfaces or the different relative positions of the connecting loop and the α helix.

TPN_Q will be a very useful molecular probe for exploring the physiological functions and molecular mechanisms of inward-rectifier K^+ channels. Knowledge of the mechanisms by which TPN_Q interacts and inhibits the channel will enhance its usefulness as a tool. In the present study, we examined the kinetics of channel inhibition by TPN_Q and channel recovery from inhibition. From these kinetic studies, we determined the channel−TPN_Q stoichiometry. Furthermore, using alanine-scanning mutagenesis, we delineated the TPN_Q receptor in the channel as well as the region of the TPN_Q surface that binds to the channel.

MATERIALS AND METHODS

Channel Expression. Oocytes harvested from *Xenopus laevis* frogs were digested with collagenase (2 mg/mL) in a solution containing 82.5 mM NaCl, 2.5 mM KCl, 1.0 mM $MgCl_2$, 5.0 mM (pH 7.6) HEPES. The oocyte digestion solution was agitated on a platform shaker at a rate of 80 rpm for 90 min. The oocytes were then rinsed thoroughly with and stored in a solution containing 50 μg/mL gentamicin, 96 mM NaCl, 2 mM KCl, 1.8 mM $CaCl_2$, 1 mM $MgCl_2$, 5 mM (pH 7.6) HEPES. Defolliculated oocytes were selected at least 2 h after the collagenase digestion. To express the ROMK1 channel, the coding RNA was directly injected into oocytes. All injections were carried out at least 16 h after the collagenase treatment. The injected oocytes were stored in a 18 °C incubator.

Channel Recording. The ROMK1 channel was studied using a two-electrode voltage clamp amplifier (Oocyte Clamp OC-725C, Warner Instruments Corp.) The resistance of electrodes filled with 3 M KCl was 0.3−0.5 MΩ. To elicit

† This study was supported by an NSF grant (IBN-97-27436). Z. Lu was a recipient of an Independent Scientist Award from NIH (HL03814).

* Please send correspondence to: Dr. Zhe Lu, University of Pennsylvania, Department of Physiology, D302A Richards Building, 3700 Hamilton Walk, Philadelphia, PA 19104. Telephone: 215-573-7711. Fax: 215-573-5851. E-mail: zhelu@mail.med.upenn.edu.

10.1021/bi991206j CCC: $18.00
Published on Web 10/09/1999

current through the channel, the membrane potential of oocytes was stepped to −80 mV and then to +80 mV from the holding potential of 0 mV. Background leak currents were obtained by exposing oocytes to solutions containing TPN_Q at concentrations greater than 100-fold of K_i. The bath solution contained 100 mM KCl, 0.3 mM $CaCl_2$, 1.0 mM $MgCl_2$, 10 mM (pH 7.6) HEPES. The concentrations of TPN_Q and its derivatives were calculated by converting the absorbance of the solution at 280 nm wavelength using an extinction coefficient 6.1 mM^{-1} cm^{-1} (*3*). In the case where W15 was replaced by an alanine residue, the concentration of the derivative was estimated by normalizing the peak area of a sample (in a predetermined volume) detected at 215 nm wavelength on HPLC to that of a known quantity of TPN_Q sample. All toxin-containing solutions were freshly made by diluting stock solutions. TPN_Q as well as its derivatives used in the experiments were made synthetically (see below).

Molecular Biology. The ROMK1 cDNA was cloned into a pSPORT plasmid (Gibco-BRL) (*9*). A mutation was introduced into the ROMK1 cDNA to create an *Nde*I site without altering the amino acid sequence. Mutations in the ROMK1 cDNA were produced using the polymerase chain reaction (PCR) primed with a mutagenic oligonucleotide. A sequenced 240-base-pair fragment, containing the mutation (between *Nde*I and *Bgl*II), was subcloned into a wild-type recipient version of the ROMK1 cDNA. The cRNA was synthesized using T7 polymerase from the cDNA linearized using *Not*I (Promega).

Synthesis, Mass Determination and Purification of Tertiapin and Its Derivatives. TPN_Q and its derivatives were synthesized using a Rainin/Protein Technologies Symphony multipeptide synthesizer, and their mass was confirmed on a VG analytical MALDI-TOF spectrometer. Unless specified, synthetic TPN_Q and all its derivatives have a C-terminal amide group. For a comparative purpose, TPN_Q with a C-terminal free carboxyl group was synthesized. All the synthetic peptides spontaneously adopted the correct conformation in a solution containing 1 mM DTT and 10 mM Tris (pH 8.0) after DTT became oxidized (*3*). After the peptides folded into the correct conformation, they were purified with a reverse phase HPLC column (C18) using a linear methanol gradient (1% per minute). The flow rate was 1 mL/min.

RESULTS

Delineation of the TPN_Q Receptor in the ROMK1 Channel through Alanine-Scanning Mutagenesis. Earlier studies showed that some mutations in the M1−M2 linker of the ROMK1 channel affect TPN binding (*3*). In contrast, the N171D mutation in the M2 region does not significantly affect the channel-toxin interaction (*3*), despite the fact that the N171D mutation dramatically increases the channel affinity for intracellular cationic blockers, such as Mg^{2+} and polyamines (*10*−*12*). Thus, it appears that the M1−M2 linker forms the TPN receptor.

To identify *potential* interaction residues in the M1−M2 linker and thus delineate the toxin receptor, we replaced all the residues in the M1−M2 linker, one at a time, with alanine or valine when the native residue is alanine (*13*). Figure 1A−F shows current traces of the wild-type and five representative mutant ROMK1 channels in the absence and presence of TPN_Q at the concentrations indicated. TPN_Q at a concentration of 2 nM inhibited a little more than half of the current of the ROMK1 channel. Alanine mutation at residues D116 and F146 dramatically reduced channel affinity for TPN_Q, resulting in an 8- and 50-fold higher concentration requirement to inhibit half of the current. On the other hand, the alanine mutation at P120 enhanced channel affinity for TPN_Q, seen as a 15-fold reduction in the concentration of TPN_Q required to inhibit half of the current. In contrast, alanine mutations at some other channel residues, e.g., residues M128 and Q152, had little effect on channel affinity for TPN_Q.

The fractions of unblocked currents through the wild-type and five mutant channels were plotted against the concentration of TPN_Q in Figure 1G. To determine the K_i values for each channel, we fit the data with an equation that assumes the stoichiometry between the channel and TPN_Q is one-to-one (see below). The analyses confirm that mutant channels M128A and Q152A have affinities for TPN_Q similar to that of the wild-type channel, the P120A channel has a 15-fold higher affinity, while the D116A and F146A channels have 8- and 50-fold lower affinities for TPN_Q.

To summarize the effects of channel mutations on TPN_Q binding, we plotted the ratios of K_i values of the mutant channels and the wild-type channel (in the natural logarithm form) against the primary sequence of the M1-M2 linker in Figure 2. At many residue positions, e.g., from 131 to 145, no data were presented because the cRNAs containing the corresponding mutations did not express any detectable ionic currents. As shown in Figure 2, mutations at most residues from 114 to 123 as well as at residues 146 and 148 significantly affect the binding of TPN_Q.

Identification of the TPN_Q Interaction Surface through Alanine-Scanning Mutagenesis. To identify the *potential* interaction residues in TPN_Q and thus delineate its interaction surface, we replaced each TPN_Q residue, except for the four cysteine, one at a time, with alanine or valine when the native residue is alanine. Figure 3A−F shows current traces of the ROMK1 channel in the absence and presence of TPN_Q and five representative derivatives. Much higher concentrations of TPN_Q derivatives, containing alanine at residues H12, K17, and K20, than that of TPN_Q itself, were required to inhibit half of the ROMK1 current. Thus, alanine substitution at these three TPN_Q residues dramatically affects the binding of TPN_Q to the channel. In contrast, alanine mutation at residue L2 had almost no effect on the binding of TPN_Q to the channel, while alanine mutation at residue I9 slightly enhanced TPN_Q binding.

The fraction of unblocked ROMK1 currents by TPN_Q and the five TPN_Q derivatives were plotted against their concentration in Figure 3G. Again, to determine the K_i values of the channel for TPN_Q and its derivatives we fit the data using an equation assuming a one-to-one stoichiometry between TPN_Q and the channel. The analyses show that the channel binds the TPN_Q derivative with alanine substitution at residue L2 with a K_i value nearly identical to that of TPN_Q and binds the one with alanine mutation at I9 with a 2-fold lower K_i. Comparatively, when the channel binds to the TPN_Q derivatives with alanine substitution at residues H12, K17, and K20, the K_i values are 20-, 5- and 15-fold higher, respectively.

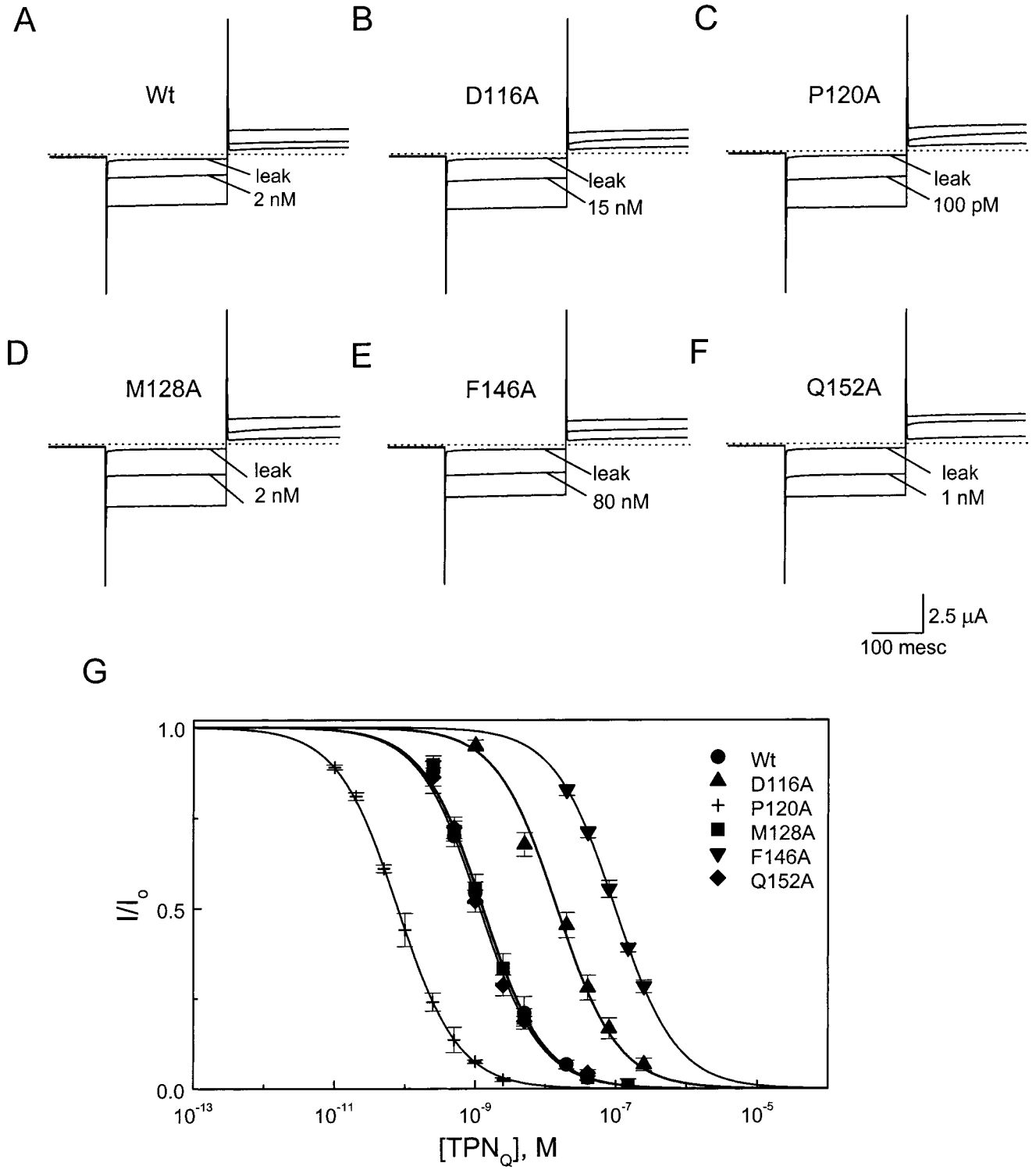

FIGURE 1: Inhibition of the wild-type and mutant ROMK1 channels by TPN_Q. A−F: Current traces of the wild-type and five representative mutant ROMK1 channels in the absence and presence of TPN_Q at concentrations indicated. The leak current traces were obtained in the presence of TPN_Q at concentrations greater than 100 times of the corresponding K_i values. The dotted lines identify the zero current level. G: The fraction of unblocked currents (mean ± sem, $n = 4-50$) for each of the six channels were plotted as a function of the concentration of TPN_Q. The curves superimposed on the data points are the fits of an equation $I/I_o = K_i/(K_i + [TPN_Q])$.

The effects of all alanine mutations in TPN_Q are summarized in Figure 4, where we plotted the K_i value ratios between TPN_Q derivatives and TPN_Q itself (in a natural logarithm term) against the primary sequence of TPN_Q. The data reveal an interesting pattern: alanine mutations at the eight noncysteine residues within the C-terminal half dramatically affect the channel-toxin interaction, whereas the mutations at the nine noncysteine resides within the N-terminal half of the peptide had no or a much smaller effect (Figure 4).

Amidation occurs at the C-terminus of TPN as well as many other proteins purified from honey bee venom. Generally speaking, amidation of many proteins is critical for the biological activity. To examine whether the C-

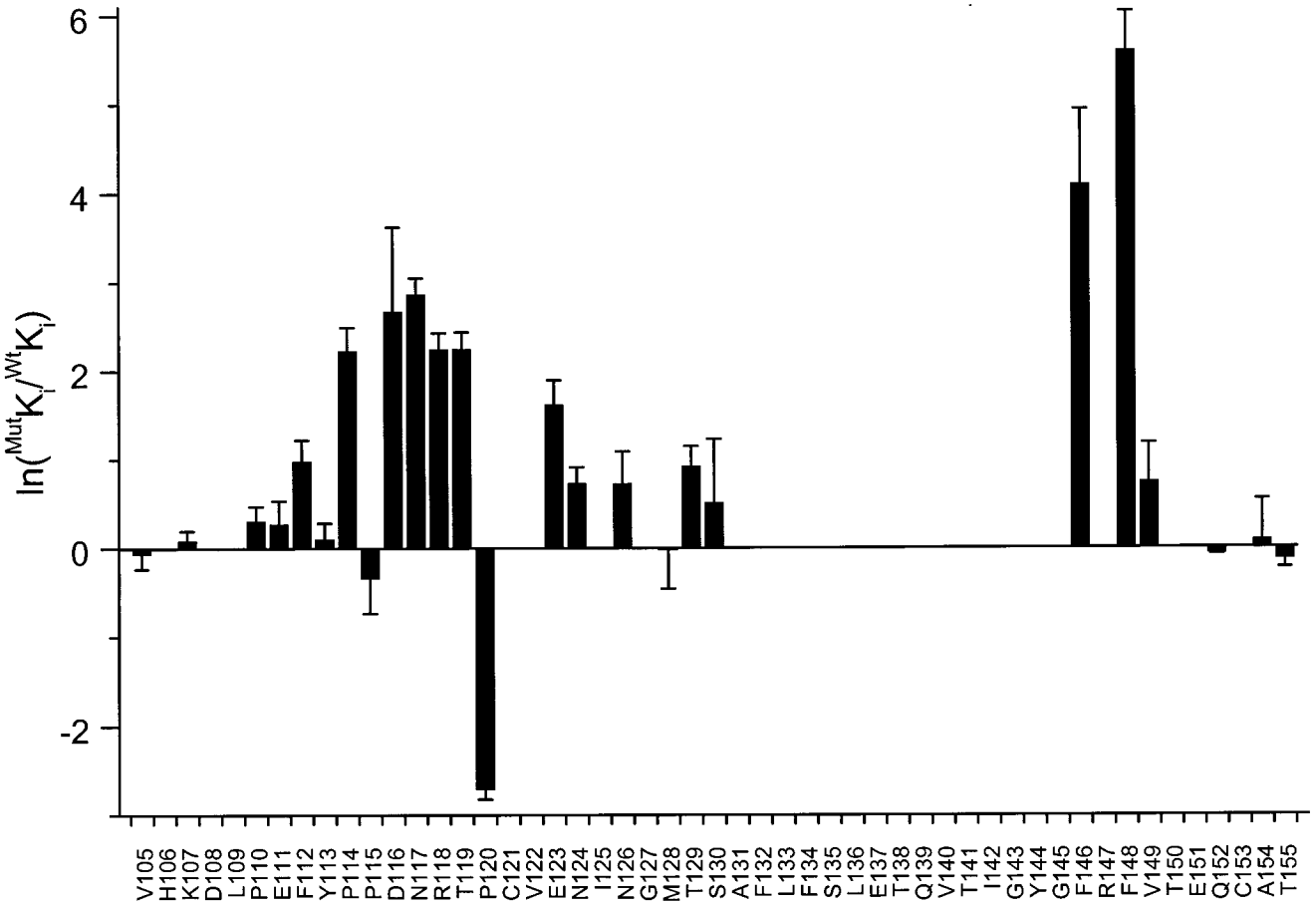

FIGURE 2: Effects of mutations in the M1−M2 linker of ROMK1 on TPN_Q binding. The natural logarithm of the relative K_i values between the mutant and the wild-type channel (mean ± sem, $n = 3-50$) were plotted against the primary sequence of the M1−M2 linker. Each of the residues in the M1−M2 linker was substituted with alanine or valine when the native residue is alanine. A lack of data at many residue positions is because the cRNAs containing the corresponding mutations did not express any detectable ionic currents.

terminal amide in TPN_Q plays a critical role in its interaction with the channel, we compared the blocking activity of TPN_Q with a C-terminal amide (TPN_Q−AM) versus a free carboxyl acid (TPN_Q−CA). Figure 5, A and B, shows the current traces of the ROMK1 channel in the absence or presence of TPN_Q−AM and TPN_Q−CA, respectively. The fraction of unblocked current was plotted against the concentration of TPN_Q−AM and TPN_Q−CA in Figure 5C. The curves superimposed on the data points correspond to the fits of an equation assuming that one TPN_Q molecule blocks one channel. The results of the fits indicate that the affinity of the channel for TPN_Q−AM is only about 2-fold higher than that for TPN_Q−CA. Thus, the C-terminal amidation in TPN_Q has a small effect on its binding to the ROMK1 channel.

Kinetics of Channel Inhibition by TPN_Q. The rate constant for TPN_Q (and TPN) binding to the ROMK1 channel is rather large. Consequently, the rates of channel inhibition by TPN_Q at the concentrations producing measurable channel inhibition were too fast to be accurately determined because of the relative slow rate of solution exchange over the entire oocyte surface membrane. Fortunately, we found a mutant channel, P120A, that binds to TPN_Q with a 15-fold higher affinity ($K_i = 80$ pM) than the wild-type channel (Figures 1 and 2). The inhibition rates of this mutant channel by TPN_Q at 20−500 pM were slow enough for us to determine accurately. In this concentration range, TPN_Q inhibited 20−85% of the P120A channels.

As shown in Figure 6A, the time course of current change upon washing-in and washing-out of TPN_Q (250 pM) can be well-fit with single-exponential functions. In Figure 6B, we plot the reciprocals of the time constants for channel inhibition upon washing-in of TPN_Q ($1/\tau_{on}$) and its recovery upon washing-out ($1/\tau_{off}$) against the concentration of TPN_Q. The plot shows that $1/\tau_{on}$ depends linearly on TPN_Q concentration and $1/\tau_{off}$ is independent of the concentration. These findings argue for a one-to-one stoichiometry between TPN_Q and the channel. In this case, $1/\tau_{on} = k_{on}[TPN_Q] + k_{off}$ and $1/\tau_{off} = k_{off}$, where k_{on} and k_{off} are the rate constants for TPN binding and unbinding, and $[TPN_Q]$ is the concentration of TPN_Q. From the slope of a linear fit of $1/\tau_{on}$ versus $[TPN_Q]$ we obtained $k_{on} = 3.0 \times 10^8\ M^{-1}\ s^{-1}$, and from the averaged $1/\tau_{off}$, we obtained $k_{off} = 2.4 \times 10^{-2}\ s^{-1}$. The K_i value of 80 pM calculated from k_{off}/k_{on} agrees with that determined from the equilibrium measurement (80 pM).

DISCUSSION

TPN_Q, a nonair oxidizable derivative of tertiapin, inhibits the ROMK1 channel with nanomolar affinity (*4*). One way to determine the stoichiometry between the channel and TPN_Q is from the kinetics of their interaction (e.g., ref *14*). However, the rate constant for TPN_Q (and TPN) binding to the channel is unusually large, making it difficult for us to examine the kinetics of their interaction. To overcome this

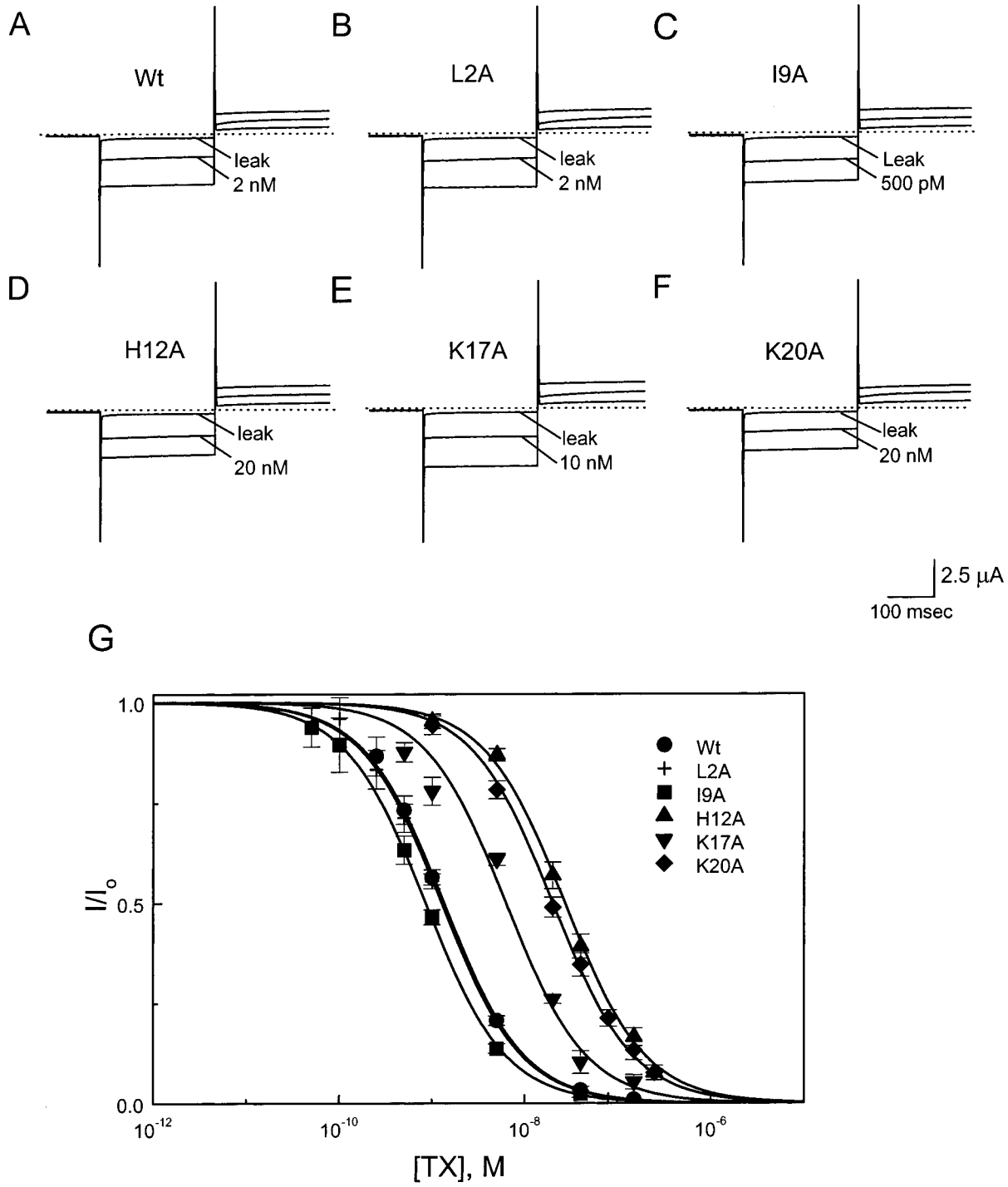

FIGURE 3: Inhibition of the ROMK1 channel by TPN_Q and its derivatives. A−F: Current traces of the ROMK1 channel in the absence and presence of TPN_Q and five of its derivatives at the concentrations indicated. The leak current traces were obtained in the presence of TPN_Q at concentrations greater than 100 times of the K_i value. The dotted lines identify the zero current level. G: The fractions of unblocked currents (mean ± sem, $n = 3-50$) of the ROMK1 channel were plotted as a function of the concentration of TPN_Q and five of its derivatives. The curves superimposed on the data points are the fits of an equation $I/I_o = K_i/(K_i + [TX])$.

difficulty, we used a high-affinity ROMK1 mutant channel with its P120 replaced by an alanine residue. The P120A channel has a 15-fold higher affinity for TPN_Q, thus 15-fold lower concentrations of TPN_Q produce resolvable channel inhibition (> 20%) (Figures 1 and 2). At lower concentrations of TPN_Q, the rates of channel inhibition were more than 10-fold slower. Compared to the wild-type channel, the recovery rate of the P120A channel from TPN_Q inhibition was also significantly reduced. Thus, we were able to carefully examine the kinetics of the channel-TPN_Q interaction at TPN_Q concentrations between 20 and 500 pM.

The rate of TPN_Q binding to the channel depends linearly on the concentration of TPN_Q, whereas the rate of TPN_Q unbinding is independent of the concentration (Figure 6). These results argue strongly that the interaction between the channel and TPN_Q is a bimolecular reaction, and thus the stoichiometry between them is one-to-one. Certainly, the value of the rate constant for TPN_Q binding to the channel,

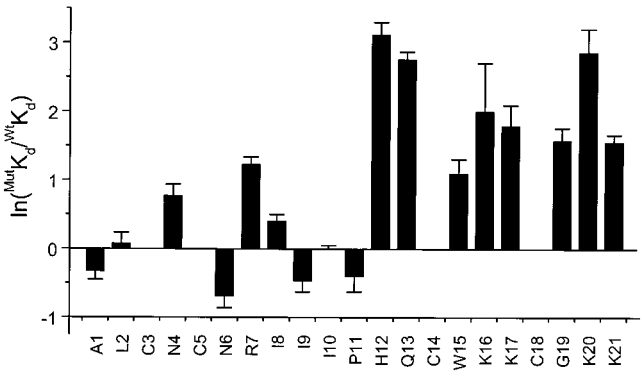

FIGURE 4: Effects of mutations in TPN_Q on its interaction with the ROMK1 channel. Natural logarithm of the relative K_i values between TPN_Q derivatives and TPN_Q (mean ± sem, $n = 3-50$) were plotted against the primary sequence of TPN_Q. Each residue in TPN_Q, except for the four cysteine residues, was substituted with alanine or valine when the native residue is alanine.

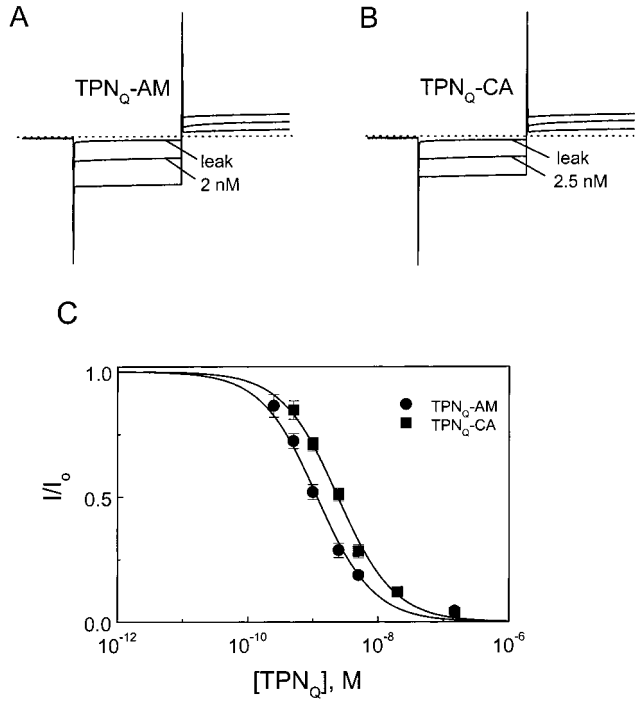

FIGURE 5: The effect of C-terminal amidation on the binding of TPN_Q to the channel. A and B: ROMK1 current traces in the absence or presence of either TPN_Q−AM and TPN_Q−CA, respectively. C: The fractions of unblocked currents (mean ± sem, $n = 4-50$) were plotted against the concentration of TPN_Q−AM and TPN_Q−CA, respectively. The curves superimposed on the data points correspond to an equation of $I/I_o = K_i/(K_i + [TPN_Q])$. The fits yield that K_i values of 1.3 ± 0.1 (mean ± sem) nM and 2.4 ± 0.7 nM for TPN_Q−AM and TPN_Q−CA, respectively.

3.0×10^8 M^{-1} s^{-1}, is unusually large for a protein−protein interaction. However, a precedence for such a large binding rate constant (2.1×10^8 M^{-1} s^{-1}) has been reported for the binding of a scorpion toxin (AgTx2) to a voltage-activated K^+ channel (K_V1.3) (*29*). Since TPN_Q has a high density of positively charged residues (four lysine, one arginine, and one histidine), the large TPN_Q binding constant is likely augmented by some electrostatic interactions between the channel and the toxin.

The results from the mutagenesis study on TPN_Q indicate that the secondary structure underlying its interaction surface is fundamentally different from those of scorpion toxins.

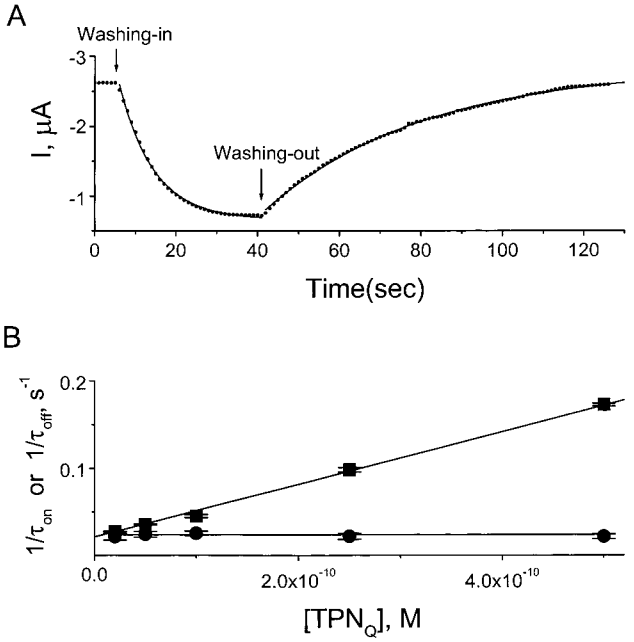

FIGURE 6: Inhibition kinetics of the P120A mutant ROMK1 channel by TPN_Q. A: Time courses of current changes upon washing in and washing out TPN_Q (250 pM). The interval between two adjacent data points is one second. The curves superimposed on the data points correspond to the fits using single-exponential functions. The fits yield that $\tau_{on} = 8.5$ s and $\tau_{off} = 38.9$ s. B: The reciprocals of the time constants (mean ± sem, $n = 13-24$) for washing in ($1/\tau_{on}$; squares) and washing out ($1/\tau_{off}$; closed circles) TPN_Q are plotted as a function of TPN_Q concentration. The lines superimposed on the data points are the fits using functions $1/\tau_{on} = k_{on}$ [TPN_Q] + k_{off} and $1/\tau_{off} = k_{off}$, respectively. The fits yield that $k_{on} = 3.01$ (± 0.02) × 10^8 M^{-1} s^{-1} [mean (± sem)] and $k_{off} = 2.4$ (± 0.4) × 10^{-2} s^{-1}.

Charybdotoxin and other related scorpion toxins consist of a triple-stranded β sheet and an α helix (*15*−*19*). The surface with which scorpion toxins binds to targeted channels—the interaction surface—is primarily formed by the residues in the β strands. Comparatively, bee toxins, such as TPN, also consist of an α helix formed by the C-terminal half of the peptide and some extended structures formed by the N-terminal half (ref 8; also see Figure 7A). Alanine mutations at the residues in the α helix dramatically impair TPN_Q binding, whereas those in the extended structures had no or a much smaller effect (Figure 4). These results argue strongly that the interaction surface of TPN_Q is primarily formed by the α helix rather than the extended structures as in scorpion toxins. Figure 7C is a space-filled model of TPN with the same orientation shown in Figure 7A. The bottom surface is shown in Figure 7, B and D, obtained by a 90° rotation of the models in Figure 7, A and C around a horizontal axis in the forward direction, respectively. Figure 7, C and D, clearly illustrates that all of the residues in the α helix critical for the ROMK1-TPN_Q interaction are located on this surface. Many noncysteine residues in the α helix critical for the ROMK1−TPN_Q interaction are not conserved in apamin and mast cell degranulating peptide (MCDP) (Figure 7E). Thus, it is understandable why these two bee toxins do not block the channel with high affinity (*3*), despite the fact that the bee toxins have very similar three-dimensional backbone structures (*7*, *8*).

Many mutations in the M1−M2 linker of ROMK1, forming the external part of the ion conduction pore, affect

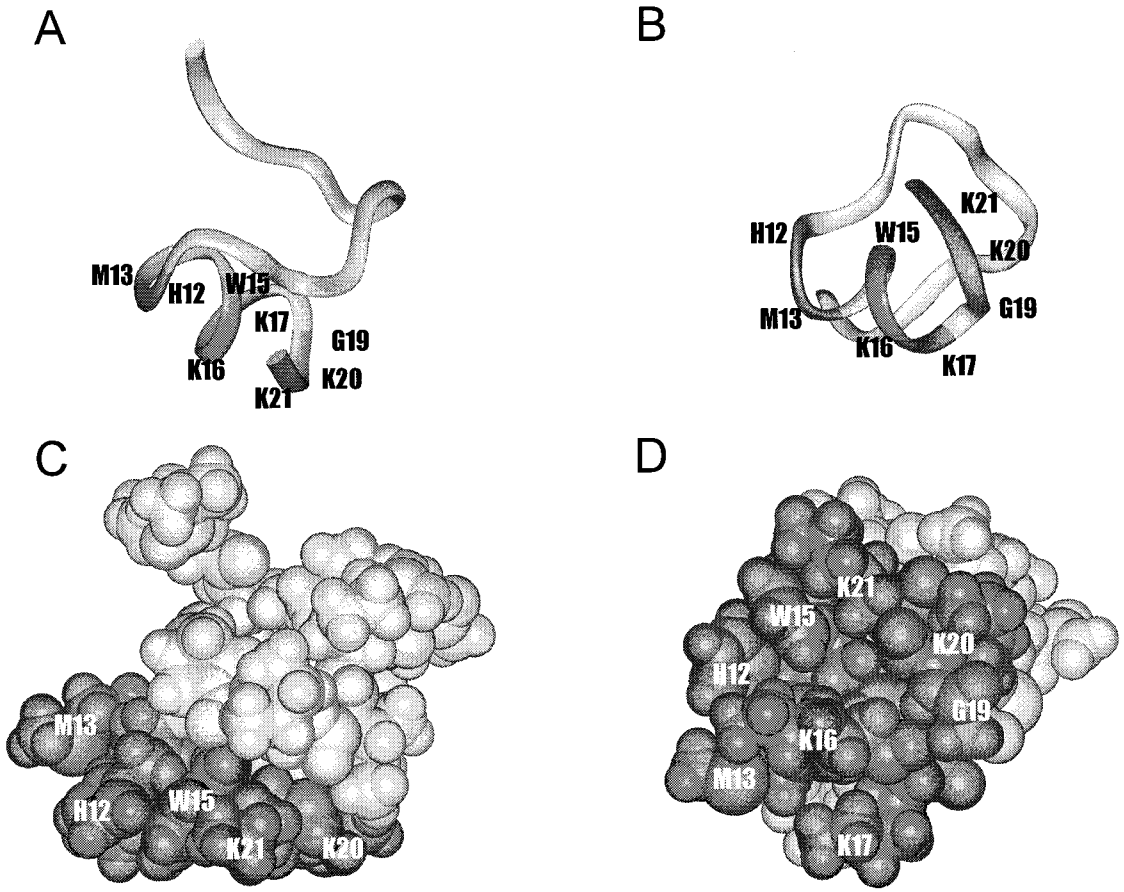

E

```
Tertiapin      A L C N C N R - I I I P H M C W K K C G K K
Apamin           C N C K - - A P E T A L C A R R C Q Q H
MCD Peptide    I K C N C K R H V I K P H I C R K I C G K N
```

F

			Turret	Pore Helix	Selectivity Filter	
KcsA	M1--	(51)	ERGAPGAQLITYPRALWWSVETATTVGYGDLYPVTL			(86)--M2
Shaker	S5--	(418)	EAGSENSFFKSIPDAFWWAVVTMTTVGYGDMTPVGVWGKI			(457)--S6
ROMK1	M1--	(106)	HKDLPEFYPPDNRTPCVENINGMTSAFLFSLETQVTIGYGFRFVTEQCAT			(155)--M2

FIGURE 7: NMR structural model of TPN (*8*), amino acid sequence alignment among three bee toxins and partial amino acid sequence alignments of three K^+ channels. A and C: Ribbon and space-filled models of TPN structure in the same orientation. B and D: Ribbon and space-filled models of TPN obtained by rotating forward the models in A and C around the horizontal axis 90°. E: Amino acid sequence alignment of TPN, apamin, and mast cell degranulating peptide. F: Amino acid sequence alignment of the M1−M2 (or S5−S6) linkers in the KcsA, *Shaker*, and ROMK1 channels using the signature sequence as a reference.

the interaction between the channel and TPN_Q (Figure 2). Although different classes of K^+ channels may have some differences in their structures (*20*), a similar pattern exits when the mutagenesis data from the current study on TPN_Q−ROMK1 interaction are compared with those from previous studies on the interaction between pore-blocking scorpion

toxins and voltage-activated K^+ channels (*21*−*34*). In both cases, mutations affecting channel-toxin interaction are at those N-terminal residues in the S5−S6 (equivalent to M1−M2) linker and also those residues C-terminal to the signature sequence that forms the narrow and selective part of the pore (*35*, *36*). Mutagenesis studies in the voltage-activated K^+ channels suggest that the residues in these two regions form the external vestibule of the K^+ pore. Subsequent comutagenesis (in both the voltage-activated K^+ channels and scorpion toxins) studies, aided by thermodynamic mutant cycle analysis, led to the identification of the residue pairs at the channel−toxin interface (*23*−*34*). Using the toxins of known structure as templates, each identified channel residue pairing with a toxin residue was assigned a location in space (*30*−*33*). The number of channel residues that could be assigned was limited. However, the residues that were assigned clearly delineated the molecular architecture of the external vestibule of the K^+ pore (*30*−*33*). In fact, both the predicted architecture for the vestibule and the residue assignments in those studies are remarkably compatible with the structure of a bacterial K^+ channel (KcsA), recently solved at a 3.4 Å resolution using X-ray diffraction techniques (*36*). Furthermore, the crystallographic structural model of the KcsA channel provides the structural basis for us to appreciate in detail how scorpion toxins interact with K^+ pores and why mutations in certain regions affect their interaction (*36*, *37*).

The crystallographic structural model of the KcsA channel shows that the signature sequence forms the narrow region of the K^+ pore (*36*, also see Figure 7F). The residues C-terminal to the signature sequence forms the base of the external vestibule of the K^+ pore, while the N-terminal part of the M1−M2 linker forms four turrets around the pore to line up the vestibule. When a scorpion toxin binds to the K^+ pore, the middle portion of the toxin contacts the base of the vestibule, while its two ends are in contact with the turrets (*37*), which explains why mutations at the turret- and vestibule base-forming residues affect the binding of scorpion toxins to the voltage-activated K^+ channels.

Here, we also observed that alanine mutations at many residues (114−123, 146, and 148) forming the external vestibule of the ion conduction pore affect the binding of TPN_Q to the ROMK1 channel (Figures 2 and 7F). Furthermore, the mutations in the C-terminal α-helix not the N-terminal extended structures dramatically affect TPN_Q−ROMK1 interaction. These results allow one to envision that to block the K^+ pore TPN_Q plugs its α helix into the vestibule of the K^+ pore, while leaving its extended structural portion sticking out of the vestibule into the extracellular media. The protruding "tail" is a perfect place to put desirable labels on TPN_Q that can in turn be used to label the targeted channels.

ACKNOWLEDGMENT

We thank K. Ho and S. Hebert for the ROMK1 cDNA clone, C. Deutsch for critical reading of our manuscript, and J. Rush for a helpful discussion. Mass spectrometry and peptide synthesis were performed at the Biopolymer Facility, Harvard Medical School.

REFERENCES

1. Gauldie, J., Hanson, J. M., Rumjanek, F. D., Shipolini, R. A., and Vernon, C. A. (1976) *Eur. J. Biochem. 61*, 369−376.
2. Ovchinnikov, Y. A., Miroshnikov, A. I., Kudelin, A. B., Kostina, M. B., Boikov, V. A., Magzanik, L. G., and Gotgilf, I. M. (1980) *Bioorg. Khim. 6*, 359−365.
3. Jin, W., and Lu, Z. (1998) *Biochemistry 38*, 13291−13299.
4. Jin, W., and Lu, Z. (1999) *Biochemistry, 38*, 14286−14293.
5. Blatz, A. L., and Magleby, K. L. (1986) *Nature 323*, 718−720.
6. Stuhmer, W., Ruppersburg, J. P., Schroter, K. H., Sakmann, B., Stocker, M., Giese, K. P., Perschke, A., Baumann, A., and Pongs, O. (1989) *EMBO J. 8*, 3235−3244.
7. Pease, J. H., and Wemmer, D. E. (1988) *Biochemistry 27*, 8491−8498.
8. Xu, X., and Nelson, J. W. (1993) *Protein: Struct., Funct., Genet. 17*, 124−137.
9. Ho, K., Nichols, C. G., Lederer, W. J., Lytton, J., Vassilev, P. M., Kanazirska, M. V., and Hebert, S. C. (1993) *Nature 362*, 127−132.
10. Lu, Z., and MacKinnon, R. (1994) *Nature 371*, 243−246.
11. Wible, B. A., Taglialatela, M., Ficker, E., and Brown, A. M. (1994) *Nature 371*, 246−249.
12. Lopatin, A. N., Makhaina, E. N., and Nichols, C. G. (1994) *Nature 372*, 366−369.
13. Clackson, T., and Wells, J. A. (1995) *Science 267*, 383−386.
14. Giangiacomo, K. M., Garcia, M. L., and McManus, O. B. (1992) *Biochemistry 31*, 6719−6727.
15. Bontems, F., Gilquin, B., Roumestand, C., Menez, A., and Toma, F. (1992) *Biochemistry 31*, 7656−7764.
16. Johnson, B. A., and Sugg, E. E. (1992) *Biochemistry 31*, 8151−8159.
17. Johnson, B. A., Scott, P. S., and Williamson, J. M. (1994) *Biochemistry 33*, 15061−15070.
18. Krezel, A. M., Kasibhatla, C., Hidalgo, P., MacKinnon, R., and Wagner, G. (1995) *Protein Sci. 4*, 1478−1489.
19. Renisio, J.-G., Lu, Z., Blanc, E., Jin, W., Lewis, J. H., Bornet, O., and Darbon, H. (1999) *Proteins: Struct., Funct., Genet. 34*, 417−426.
20. Minor, D. L., Jr., Masseling, S. J., Jan, Y. N., and Jan L. Y. (1999) *Neuron 96*, 879−891.
21. MacKinnon, R., and Miller, C. (1988) *J. Gen. Physiol. 91*, 335−349.
22. Miller, C. (1988) *Neuron 1*, 1003−1006.
23. Park, C.-S., and Miller, C. (1992) *Neuron 9*, 307−313.
24. MacKinnon, R., and Miller, C. (1989). *Science 245*, 1382−1385.
25. MacKinnon, R., Heginbotham, L., and Abramson, T. (1990) *Neuron 5*, 767−771.
26. Stampe, P., Kolmakova-Partensky, L., and Miller, C. (1994) *Biochemistry 31*, 443−450.
27. Goldstein, S. A. N, Pheasant, D. J., and Miller, C. (1994) *Neuron 12*, 1377−1388.
28. Stocker, M., and Miller, C. (1994) *Proc. Natl. Acad. Sci. U.S.A. 91*, 9509−9513.
29. Gross, A., Abramson, T., and MacKinnon, R. (1994) *Neuron 13*, 961−966.
30. Hidalgo, P., and MacKinnon, R. (1995) *Science 268*, 307−310.
31. Aiyar, J., Withka, J. M., Rizzi, J. P., Singleton, D. H., Andrews, G. C., Lin, W., Boyd, J., Hansoon, D. C., Simon, M., Dethlets, B., Lee, C. L., Hall, J. E., Gutman, G. A., and Chandy, K. G. (1995) *Neuron 15*, 1169−1181.
32. Rangananthan, R., Lewis, J. H., and MacKinnon, R. (1996) *Neuron 16*, 131−139.
33. Naranjo, D., and Miller, C. (1996) *Neuron 16*, 123−130.
34. Gross, A., and MacKinnnon, R. (1996) *Neuron 16*, 399−406.
35. Heginbotham, L., Lu, Z., Abramson, T., and MacKinnon, R. (1994) *Biophys. J. 66*, 1061−1067.
36. Doyle, D., Cabral, J. M., Pfuetzner, R. A., Kuo, A., Gulbis, J. M., Cohen, S. L., Chait, B. T., and MacKinnon, R. (1998) *Science 280*, 69−77.
37. MacKinnon, R., Cohen, S. L., Kuo, A., Lee, A., and Chait, B. T. (1998) *Science 280*, 106−109.

BI991206J